LTI energy-maximising control for the Wave Star wave energy converter: identification, design, and implementation

Available online at www.sciencedirect.com

ScienceDirect

IFAC PapersOnline CONFERENCE PAPER ARCHIVE

IFAC PapersOnLine 53-2 (2020) 12313–12318

LTI energy-maximising control for the Wave Star wave energy converter: identification, design, and implementation ⋆

Demián García-Violini [*,**] **Yerai Peña-Sanchez** [*]
Nicolás Faedo [*] **Christian Windt** [*] **John V. Ringwood** [*]

[*] *Centre for Ocean Energy Research, Maynooth University, Co. Kildare, Ireland.*
[**] *Universidad Nacional de Quilmes, Departamento de Ciencia y Tecnología, Bernal, Buenos Aires, Argentina. (e-mail: demian.garciaviolini@mu.ie)*

Abstract: Considering the Wave Star wave energy converter (WEC), which is a standard point absorber prototype, this study addresses the complete energy maximising control design procedure. The WEC model is obtained using system identification routines. Then, using the identified model, a LTI energy maximising control strategy, recently presented in the literature, is designed. Additionally, for the wave excitation force estimation, a standard Kalman filter with a harmonic oscillator is considered. Finally, for the assessment of the performance of the complete system, the controller and estimator are implemented in the numerical WEC simulation environment WEC-Sim. The system is tested under realistic conditions and satisfying performance of the LTI controller is shown. Thus, through a non-conventional approach, and considering a realistic software environment, a novel energy maximising controller is implemented, obtaining results which indicate the feasibility of the approach.

Keywords: Wave energy, System Identification, Energy Maximising Control, Simulation

1. INTRODUCTION

The energy of ocean waves represents a significant resource which, efficiently harvested, can make a significant contribution to the global renewable energy market (Ringwood et al., 2014). Nonetheless, the current costs of wave energy, driven by the cost of device manufacturing, deployment, operation, maintenance, and decommissioning, prevent wave energy from being competitive with other (renewable) energy sources (Korde and Ringwood, 2016). Energy maximising control strategies (EMCSs), applied to wave energy converters (WECs), can play a decisive role in reducing the cost of energy from ocean waves and, thereby, achieve commercial viability of wave energy technology.

The efficacy of model–based EMCSs is directly affected by the accuracy of the WEC model used during the design stage of the controller. In general, WEC models can be divided into two categories, either based on: (a) modelling, or (b) system identification (Ljung, 1999). EMCSs, based on physical models, are predominant in the wave energy field; however, due to unmodelled dynamics (e.g. hydrodynamic and mechanical non-linearities or may also be unmodelled high frequency linear dynamics), the robustness of these EMCSs is challenged (Ringwood et al., 2019). An example of control strategies applied to WECs based on physical modelling can be found in (Hansen and Kramer, 2011).

EMCSs, based on system identification, can be divided into two subcategories: (b.i) *grey-box-identification*, and (b.ii) *black-box-identification*. *Grey-box-identification*, employs a model structure, inspired by physical considerations, for which the system parameters are tuned using observed data, stemming e.g. from experimental studies. When the model structure is unknown and the identification is completely based on observed data (only considering general assumptions as, for example, linearity), the approach is known as *black-box-identification*. Generally, a black-box methodology allows for a more accurate model description and, consequently, more efficient controller designs. Examples of identification approaches applied in the wave energy field can be found in (Beatty et al., 2015), and (Giorgi et al., 2019).

This study presents an identification, design, and implementation procedure for the recently proposed linear time invariant controller (LiTe-Con) (García-Violini et al., 2019), applied to the Wave Star WEC (Wave Star, 2019). The LiTe-Con is tuned to approximate the frequency domain energy maximising optimal condition given by the panchromatic (broadband) impedance-matching principle, providing a broadband energy maximising control method. For WEC model characterisation, a *black-box-identification* methodology is employed, for which the observed data is extracted from a validated numerical model, based on the WEC-Sim modelling framework (WEC-Sim, 2019; Tom et al., 2018). Additionally, based on the identified model, a Kalman filter is designed for wave excitation force estimation, which is an input to the LiTe–

⋆ This material is based upon work supported by Science Foundation Ireland under Grant no. 13/IA/1886.

10.1016/j.ifacol.2020.12.1193

Con. Finally, for the assessment of the performance of the LiTe–Con, the controller is implemented in the numerical WEC-Sim model, and the absorbed energy is computed for various sea states. The identification, design, and implementation procedure, used in this study, is presented in a general form, such that its application is not restricted to the employed model or observed data, which could stem from experimental studies or, as in this case, numerical models. Regarding the control approach, in (Bacelli et al., 2019) an EMCS is proposed which, similarly to the LiTe-Con controller, is essentially an impedance-matching-based EMCS. However, unlike the LiTe-Con controller, the strategy proposed in (Bacelli et al., 2019), is presented in the feedback form and does not consider constraints.

The remainder of this paper is organised as follows. Section 2 describes the numerical modelling framework, as well as the WEC system. Section 3 details the identification methodology to identify the force–to–position and force–to–velocity mappings. In Section 4, the LiTe-Con (Section 4.1) and the estimator design (Section 4.2) are presented. The implementation of the controller is then discussed in Section 5, and the controller performance is assessed in Section 6. Finally, conclusions are drawn in Section 7.

2. SIMULATION ENVIRONMENT AND SYSTEM DESCRIPTION

This section briefly describes the WEC-Sim modelling framework and the WEC system considered herein.

2.1 WEC-Sim

To model the wave–structure interaction (WSI) between the incident wave field and a WEC structure, different numerical modelling frameworks are available (Folley, 2016). Lower-fidelity models, based on potential flow theory, are commonly applied for EMCS design, delivering solutions for the WSI at reasonable computational cost. The main underlying assumption of the employed linear hydrodynamic models are: 1) small amplitude wave and body motion; 2) incompressible, irrotational, and inviscid fluid.

WEC-Sim, developed by Sandia National Laboratories and the National Renewable Energy Laboratory, is a time-domain numerical modelling framework, solving the WSI based on Cummins' equation (1) (Cummins, 1962). WEC-Sim is implemented within MATLAB (Simulink), and allows for the inclusion of relatively accurate representations of the electro-mechanical features of the WEC device, through a coupling with the Simscape Multibody solver.

The equation of motion for a WEC can be expressed in terms of (Cummins, 1962) as [1]

$$\bar{m}\ddot{z} + \mathrm{k_R} * \dot{z} + S_\mathrm{H} z + f_\mathrm{visc} + f_\mathrm{m} = f_\mathrm{e} - f_\mathrm{u}, \qquad (1)$$

with $\bar{m} = m + A_\infty$, where m the mass of the body, A_∞ the infinite-frequency added mass. z, $\dot{z}$, and $\ddot{z}$ denote the body displacement, velocity, and acceleration, respectively. $\mathrm{k_R}$ is the radiation force impulse response and S_H the hydrostatic stiffness due to the buoyancy. The symbol $*$ is used to denote the convolution operator. The four force terms f_u, f_e, f_visc, and f_m, in Eq. (1), denote the control input, the wave excitation force, viscous forces, and mooring forces, respectively. From now on, $Z(j\omega) \leftrightarrow z(t)$ denote a Fourier transform pair.

[1] From now on, the dependence on t is dropped when clear from the context.

2.2 The Wave Star WEC

The case study considered, is based on the Wave Star WEC (Wave Star, 2019). Particularly, a 1:20th scale model of the full scale device is considered, with an electrical, direct drive, actuator PTO, inspired by the case study for the International WEC Control Competition (WECCCOMP) (Ringwood et al., 2017).

Fig. 1(a), shows a general scheme of the single floater device. Joints 1 and 3 are fixed with respect to the reference still water level (SWL). Joint 2 is mobile and has a translational displacement indicated with x_m, which represents the position of the PTO system. The device is driven by the excitation force, f_e, induced by the incident wave field.

Linear hydrodynamic effects, such as linear restoring force, linear viscous drag, and radiation force are considered in the numerical WEC-Sim model of the 1:20th scale Wave Star device. Furthermore, physical features such as the floater mass, joints, and the structural transformation due to the mobile PTO axis, are taken into account. A validation study against experimental data is presented by Tom et al. (2018).

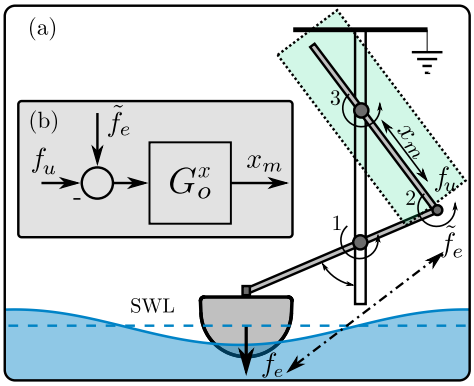

Fig. 1. (a) Full system scheme. The considered system is highlighted with the dotted green box. (b) Block diagram of the resulting force-to-motion system.

2.3 Reduced model

To avoid the representation of mechanical non-linearities in the identified model, due to the rotational DoF, only the linear displacement along the PTO axis is considered in this study. Thus, translational forces, instead of torques, are considered throughout the following sections. As a result, the WEC system can be schematically depicted as a linear translational system, subject to an excitation force $\tilde{f}_e$, representing the wave excitation force f_e acting on the device hull. For the energy maximisation control, a bi-directional external control force, f_u, is applied by means of the PTO force along the PTO axis. This reduced model is demarcated by the green-dotted box in Fig. 1(a).

Fig. 1(b) shows the block diagram used for the energy maximising control approach, in which G_o^x, assuming the principle of superposition for $\tilde{f}_e(t)$ and $f_u(t)$, represents the force-to-position mapping, considered as:

$$G_o^x(s) \equiv \begin{cases} \dot{x} = Ax + B(\tilde{f}_e - f_u), \\ x_m = Cx. \end{cases} \quad (2)$$

Since the velocity output variable is generally considered for energy maximising control problems (Falnes, 2002; Ringwood et al., 2014), note that the force-to-velocity mapping can be analytically computed using the system matrices involved in (2) as:

$$\dot{x}_m = v_m = CAx + CB(\tilde{f}_e - f_u). \quad (3)$$

3. SYSTEM IDENTIFICATION

The control design model is identified with a *black-box-identification* methodology, where the observed data are taken from the numerical WEC-Sim model. It should be noted that the following identification methodology is not restricted to observed data from numerical models only, but can also utilise experimental measurements. For the force–to–position system identification, a set of classical up-chirp experiments is performed, where the system is forced into motion by the chirp control force, while $f_e = \tilde{f}_e = 0$, i.e. no incident waves are present.

Knowing the approximate location of the natural resonance frequency of the system *a-priori*, the control force f_u is defined as linear frequency sweep in the range $[0.1, 60.0]$ rad s^{-1} (covering the resonance frequency of the system with a decade below and above), with amplitudes contained in the set $\mathcal{A} = \{2, 10, 30, 50, 60\}$ N.

Using the chirp control force and its corresponding, generated output, x_m, for each amplitude in the set $\mathcal{A}$, an empirical transfer function estimate (ETFEs), $H^x(\jmath\omega)$, are computed as follows:

$$H^x(\jmath\omega) = \frac{X_m(\jmath\omega)}{F_u(\jmath\omega)}. \quad (4)$$

Fig. 2 shows the frequency response (magnitude and phase) for each ETFE, clearly indicating linear behaviour of the system under analysis. To improve the fitting between the identified and the empirical model, the average frequency response $\bar{H}^x(\jmath\omega)$ is computed to build a low-variance set, used as the input to the frequency-domain identification algorithm (Ljung, 1999).

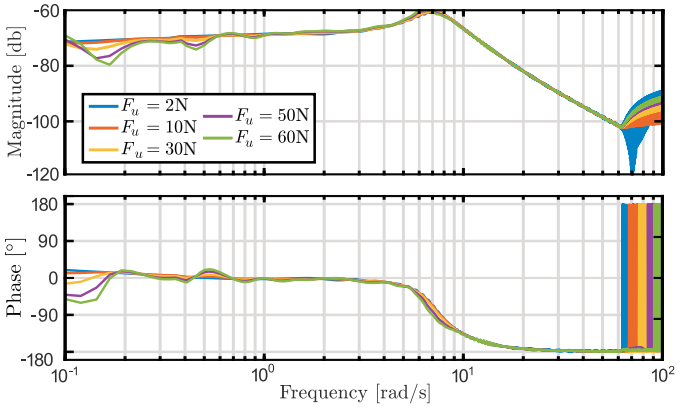

Fig. 2. Force-to-Position ETFE $H^x(\jmath\omega)$ using amplitudes 2, 10, 30, 50, and 60 N.

Considering the state-space representation of $G_o^x(s)$, the identification of the force-to-position mapping, defined in Eq. (2), is performed using subspace system identification algorithms (Ljung, 1999), which only deal with state-space system representations. Thus, using the data generated in WEC-Sim, the matrices A, B, C and D, in Eq. (2), are obtained. Thus, two sixth-order nominal linear models, G_o^x and G_o^v, are obtained for the force–to–position and force–to–velocity systems, respectively. The frequency responses of G_o^x and G_o^v are shown in Fig. 3 using solid-blue and dashed-orange lines, respectively. In addition, $\bar{H}^x(\jmath\omega)$ and $\bar{H}^v(\jmath\omega)$ are shown in Fig. 3 using dotted-light-blue and dotted-light-orange, respectively. The identification fidelity, via the normalised root mean square error, is 94.59% and 93.05% for the identification of G_o^x and G_o^v, respectively.

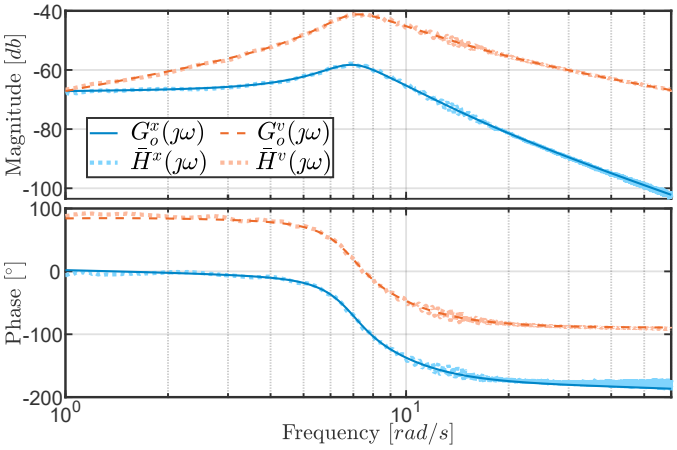

Fig. 3. Force–to–position (a) and Force–to–velocity (b) identified systems, along with the corresponding average ETFEs.

4. DESIGN

4.1 Controller Design

The LiTe-Con, proposed by García-Violini et al. (2019), is based on the fundamental requirement of impedance-matching (Falnes, 2002), but extended to the panchromatic case. Using system identification algorithms, the controller is synthesised to approximate the frequency domain energy maximising optimal condition, providing a broadband EMCS. Additionally, a suboptimal constraint handling mechanism, is implemented. While optimisation-based controllers, e.g. model predictive-based, moment-matching-based, or spectral/pseudospectral-based controllers, are predominantly used in the wave energy literature, mainly because of the optimal solutions guaranteed by these methods even in constrained scenarios, the implementation of such techniques can be challenging (Faedo et al., 2017). Conversely, in comparison with optimisation-based or non-linear controllers, the simplicity and the relatively effortless implementation of the LiTe-Con compensate for the potentially suboptimal performance. Furthermore, it is important to note that, unlike the majority of

optimisation-based control strategies, the LiTe-Con does not require forecasting of the wave excitation force.

The LiTe-Con is designed based on the force–to–velocity mapping shown in Eq. (3) and Fig. 3 with dashed-orange line. Using the real and imaginary part operators, i.e. $\mathrm{Re} : \mathbb{C} \to \mathbb{R}$ and $\mathrm{Im} : \mathbb{C} \to \mathbb{R}$, respectively, the force–to–velocity frequency-response can be expressed as:

$$G_o^v(s)\Big|_{s=\jmath\omega} = \mathrm{Re}\left\{G_o^v(\jmath\omega)\right\} + \jmath\mathrm{Im}\left\{G_o^v(\jmath\omega)\right\}. \quad (5)$$

Then, the well-known optimal feedback controller, which guarantees the impedance matching principle of optimality, is given by:

$$K_{fb}(s)\Big|_{s=\jmath\omega} = \frac{1}{\mathrm{Re}\left\{G_o^v(\jmath\omega)\right\} - \jmath\mathrm{Im}\left\{G_o^v(\jmath\omega)\right\}}. \quad (6)$$

Using Eq. (6), the optimal mapping T^{opt} from $\tilde{F}_e$ to the so-called optimal velocity profile V_m^{opt}, can be expressed, in the frequency-domain, as:

$$T^{opt}(\jmath\omega) = \frac{\mathrm{Re}\left\{G_o^v(\jmath\omega)\right\}^2 + \mathrm{Im}\left\{G_o^v(\jmath\omega)\right\}^2}{2\mathrm{Re}\left\{G_o^v(\jmath\omega)\right\}}. \quad (7)$$

Using Eqs. (5)-(7), a feedforward controller, which also guarantees the impedance matching principle of optimality, can be obtained as:

$$K_{ff}(\jmath\omega) = \frac{\mathrm{Re}\left\{G_o^v(\jmath\omega)\right\} + \jmath\mathrm{Im}\left\{G_o^v(\jmath\omega)\right\}}{2\mathrm{Re}\left\{G_o^v(\jmath\omega)\right\}}. \quad (8)$$

García-Violini et al. (2019) propose the approximation of $K_{ff}(\jmath\omega)$ with a LTI–stable and implementable dynamical system $K_{ff}^\star$, such that

$$K_{ff}^\star(s)\Big|_{s=\jmath\omega} \approx K_{ff}(\jmath\omega), \quad (9)$$

where $K_{ff}^\star$ is obtained using additional frequency-domain system identification algorithms. Then, the resulting control force (in the frequency domain) is expressed as:

$$F_u(\jmath\omega) = K_{ff}^\star(\jmath\omega)\tilde{F}_{ex}(\jmath\omega). \quad (10)$$

For further details about the LiTe-Con controller, the interested reader is referred to (García-Violini et al., 2019) where, in addition to a detailed derivation of the controller, a comparison with other well known energy maximising control strategies is presented.

The controller design results are shown in Fig. 4. The (theoretical) optimal frequency-response, $K_{ff}(\jmath\omega)$, and the achieved LiTe-Con, $K_{ff}^\star(\jmath\omega)$, frequency responses (magnitude and phase) are depicted in Fig. 4, using solid-blue and dashed-orange lines, respectively. Note that, in Fig. 4, the matching bandwidth is defined considering the sea-states shown in Section 6, Table 1.

4.2 Estimator Design

During the operation of a WEC, the wave excitation force is an unmeasurable quantity and, thus, different excitation force estimators have been proposed in the literature. Based on the comprehensive review by Peña-Sanchez et al. (2019), a standard Kalman filter, including a harmonic oscillator, is chosen for this study. This estimator features good estimation quality while inherently handling measurement noise. For the force–to–position system as

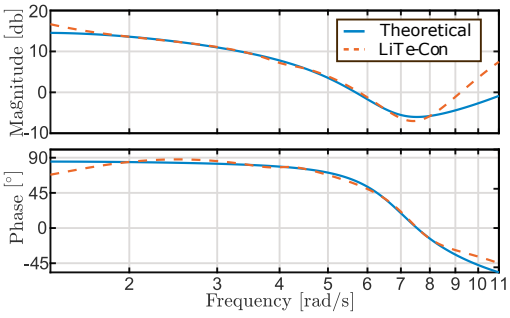

Fig. 4. Frequency responses of the theoretical optimal controller (blue) and the LiTe-Con (orange) .

defined in Eq. (2), the estimation strategy requires only position measurements of the WEC, based on the internal model principle (Goodwin et al., 2001). The dynamics of the excitation force are described, for $t \geq 0$, by the set of equations:

$$\begin{cases} \dot{x}_f = A_f x_f, \\ \tilde{f}_e = C_f x_f, \end{cases} \quad (11)$$

where the matrices A_f and C_f are defined as

$$A_f = \bigoplus_{p=1}^{\beta} \begin{bmatrix} 0 & \omega_p \\ -\omega_p & 0 \end{bmatrix}, \quad C_f = [1\ 0\ \ldots\ 1\ 0]. \quad (12)$$

where the symbol $\bigoplus$ denotes the direct sum of n matrices, i.e. $\bigoplus_{i=1}^{n} A_i = \mathrm{diag}\{A_1, A_2, \ldots, A_n\}$. Note that the matrix A_f effectively contains the set of natural frequencies chosen for the harmonic oscillator, i.e. $\{\omega_p\}_{p=1}^{\beta}$. Thus, the augmented system, required by the estimator, is given by:

$$\begin{cases} \dot{x}_a = A_a x_a - B_a f_u, \\ y = C_a x_a, \end{cases} \quad (13)$$

with

$$x_a = \begin{bmatrix} x \\ x_f \end{bmatrix}, A_a = \begin{bmatrix} A & BC_f \\ 0 & A_f \end{bmatrix}, B_a = \begin{bmatrix} B \\ 0 \end{bmatrix}, C_a = [C\ 0],$$

where the triple of matrices (A, B, C), and the state-vector x, are defined as in (2). Note that the symbol 0 indicates a zero element, dimensioned according to the context. Finally, using the augmented system matrices, an estimator gain L_K is computed as the infinite horizon Kalman gain in a standard observer form (Goodwin et al., 2001), and the excitation force can be estimated using the following observer:

$$\begin{cases} \dot{\hat{x}}_a = (A_a - L_K C_a)\hat{x}_a + [-B_a\ \ L_K]\,[f_u\ \ x_m]^\intercal, \\ \hat{\tilde{f}}_e = [0\ C_f]\,x_a. \end{cases} \quad (14)$$

By way of example, Fig. 5 shows the time response of the reference and estimated excitation forces, indicating accurate performance of the estimator. Note that the reference excitation force can be directly extracted from WEC-Sim.

5. IMPLEMENTATION

To implement the synthesised LiTe-Con in a real-time environment, or its numerical equivalent (as done here), constraint handling of the controller is essential to prevent failure of the mechanical system. García-Violini et al. (2019) propose a constraint handling mechanism, using a

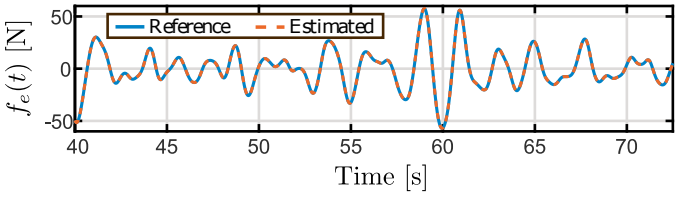

Fig. 5. Time response of the reference (blue) and estimated (dashed–orange) excitation forces.

constant $k \in [0, 1]$, so that the control force F_u in Eq. (10) is redefined as:

$$F_{uc}(\jmath\omega) = \underbrace{\left[kK^{\star}_{ff}(\jmath\omega) + (1-k)\right]}_{\text{Controller}} \hat{\tilde{F}}_{ex}(\jmath\omega), \qquad (15)$$

where it is straightforward to check that $F_{uf}(\jmath\omega) \approx F_{uc}(\jmath\omega) = \hat{F}_e(\jmath\omega)$ when $k = 0$, hence $V(\jmath\omega) \approx 0$. Assuming perfect matching in Eq. (9), the optimal mapping in Eq. (7) can be defined as:

$$T_c(\jmath\omega) = k\left(\frac{\mathrm{Re}\left\{G^v_o(\jmath\omega)\right\}^2 + \mathrm{Im}\left\{G^v_o(\jmath\omega)\right\}^2}{2\mathrm{Re}\left\{G^v_o(\jmath\omega)\right\}}\right). \qquad (16)$$

Note that, in Eq. (16), if $k = 1$, the optimal condition in Eq. (7) is obtained, i.e. $T_c(\jmath\omega) = T^{opt}(\jmath\omega)$. On the other hand, if $k = 0$, then $T_c(\jmath\omega) = 0$. Thus, the inclusion of the term k allows for the efficient implementation of position and velocity constraints between zero and their theoretical maxima. Here, the value of k is tuned using exhaustive simulation-based search, depending on each particular sea state considered (see Section 6).

To prevent negative effects on the system performance, due to estimation and controller transients, a (herein called) *transient response remover* is implemented within the LiTe-Con framework following:

$$f_{uf}(t) = (1 - e^{-\alpha t}) f_{uc}(t)\,, \qquad (17)$$

where f_{uf} denotes the actual control force applied to the system (see Fig. 7) and α is a tuning constant. Here, α is determined empirically as $\alpha = 0.1$, to smooth the first 15 seconds at the beginning of each simulation. By way of example, Fig. 6 shows the time response for the excitation force and PTO velocity for a single sea state, highlighting the effect of the transient remover. In addition, after approximately 15 seconds, it can be seen that the velocity v_m obtained using the LiTe-Con preserves *"zero-phase locking"* [2] with respect to the estimated excitation force, which is a key driver in power production with WECs (Falnes, 2002).

Fig. 7 shows the complete control structure used in this study, with the Kalman-based excitation force estimator, the constraint handling mechanism (green-dotted box), and a transient response remover (blue-dashed box).

6. CONTROLLER ASSESSMENT

In this section, simulation results for the complete control structure are shown, using the WEC-Sim modelling framework for the controller assessment. Inspired by Ringwood et al. (2017), six different, polychromatic irregular sea state (SS1–SS6) are considered for the assessment, generated from JONSWAP-based spectral density functions (Hasselmann, 1973). The significant wave height H_s, peak period T_p, and the peak shape parameter γ are listed in Table 1 for SS1–SS6. Simulations are run for 140s, and

Table 1. Sea studied used in this study

Sea State (SS)	H_s	T_p	γ
SS1	0.0208	0.988	1.0
SS2	0.0625	1.412	1.0
SS3	0.1042	1.936	1.0
SS4	0.0208	0.988	3.3
SS5	0.0625	1.412	3.3
SS6	0.1042	1.936	3.3

the absorbed energy is evaluated as:

$$E_{\text{abs}} = \frac{1}{140}\int_0^{140} f_{uf}(t)\dot{x}_m(t)\,\mathrm{dt}\,. \qquad (18)$$

The results for E_{abs} over different values of k are plotted in Figs. 8 (a)–(c), for SS1&4, SS2&5, and SS3&6, respectively.

In Figs. 8 (a)–(c), a clear trend towards increased absorbed energy, with increasing significant wave height, can be observed. Maximum absorbed energy is achieved for SS3 and SS6 with a $k \leq 0.5$. Figs. 8 (a)–(c) also clearly indicate the ability of the LiTe-Con to comply with the physical constraints of the model. While a global maximum in the absorbed energy can be observed for SS1 and SS4 with $k \approx 0.7$, the absorbed energy does not appear to have converged; however, the values for k cannot be further increased, due to the physical constraints of the device [3]. Note that the energy absorption is decreasing when $k \geq 0.7$ for SS1 and SS4, which is related to the mismatch in the controller design stage, as can be seen in Fig. 4.

7. CONCLUSION

This study presents a procedure for the identification, design, and implementation of a recently proposed EMCS for the Wave Star WEC. In the presented case study, a *black-box-identification* methodology is employed to identify the control design model (force-to-position), for which the numerical modelling framework WEC-Sim is used to generate the observed data; however, the applied methodology is presented in a general form, allowing for the use of any desired source of observed data.

The complete controller, including a Kalman–based excitation force estimator, a constraint handling mechanism, and a transient remover is assessed based on six different sea states of varying significant wave height, peak period, and peak shape parameter. The results show satisfying performance of the controller, indicating the feasibility of the proposed identification, design, and implementation procedure. However, the controller may not be as successful when the WEC system contains significant nonlinearity, or if the cost of experimental identification is prohibitive. Using experimental measurements as input to the identification methodology and, assessment of the

[2] Note that the strict-real-meaning of zero-phase-locking, only applies for monochromatic signals.

[3] Note that if k is increased beyond the limits mentioned, the device displacement would move outside the physical limits.

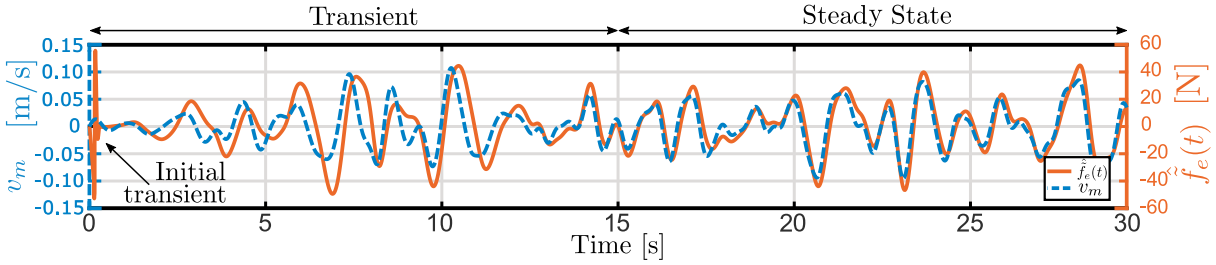

Fig. 6. Time traces of the estimated excitation force and the PTO velocity.

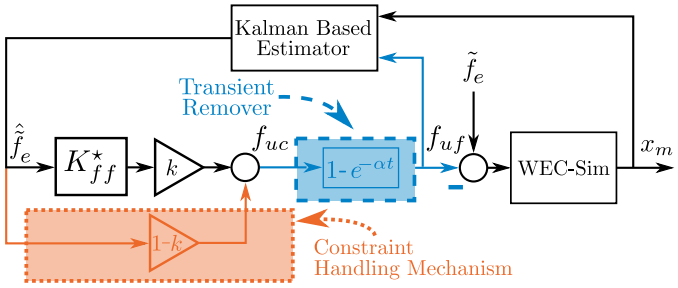

Fig. 7. Final control block diagram including the Kalman–based estimator, the constraint handling mechanism (marked in orange), and the transient remover (marked in blue).

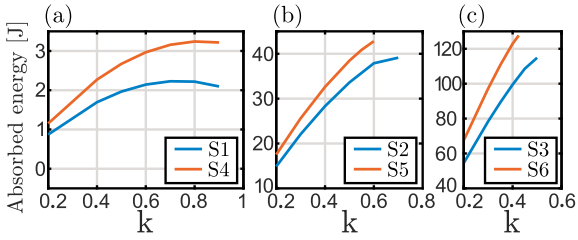

Fig. 8. Absorbed energy for different values of k for SS1&4 (a), SS2&5 (b), and SS3&6 (c).

controller in a physical environment form pertinent future work.

REFERENCES

Bacelli, G., Nevarez, V., Coe, R.G., and Wilson, D. (2019). Feedback resonating control for a wave energy converter. *IEEE Transactions on Industry Applications*, 56(2), 1862–1868.

Beatty, S.J., Hall, M., Buckham, B.J., Wild, P., and Bocking, B. (2015). Experimental and numerical comparisons of self-reacting point absorber wave energy converters in regular waves. *Ocean Engineering*, 104, 370–386.

Cummins, W.E. (1962). The impulse response function and ship motions. *Schiffstechnik*, 47, 101–109.

Faedo, N., Olaya, S., and Ringwood, J.V. (2017). Optimal control, MPC and MPC-like algorithms for wave energy systems: An overview. *IFAC Journal of Systems and Control*, 1, 37–56.

Falnes, J. (2002). *Ocean waves and oscillating systems: linear interactions including wave-energy extraction*. Cambridge University Press.

Folley, M. (2016). *Numerical modelling of wave energy converters: state-of-the-art techniques for single devices and arrays*. Academic Press.

García-Violini, D., Peña-Sanchez, Y., Faedo, N., and Ringwood, J.V. (2019). An energy-maximising linear time invariant controller (LiTe-Con) for wave energy devices. *IEEE Transactions on Sustainable Energy*.

Giorgi, S., Davidson, J., Jakobsen, M., Kramer, M., and Ringwood, J.V. (2019). Identification of dynamic models for a wave energy converter from experimental data. *Ocean Engineering*, 183, 426–436.

Goodwin, G.C., Graebe, S.F., Salgado, M.E., et al. (2001). *Control system design*, volume 240. Prentice Hall New Jersey.

Hansen, R.H. and Kramer, M.M. (2011). Modelling and control of the Wave Star prototype. In *Proceedings of the 9th European Wave and Tidal Energy Conference (EWTEC) 2011, Southampton, UK*.

Hasselmann, K. (1973). Measurements of wind wave growth and swell decay during the Joint North Sea Wave Project (JONSWAP). *Deutches Hydrographisches Institut*, 8, 95.

Korde, U.A. and Ringwood, J.V. (2016). *Hydrodynamic control of wave energy devices*. Cambridge University Press.

Ljung, L. (1999). *System Identification - Theory for the User*. Prentice Hall.

Peña-Sanchez, Y., Windt, C., Josh, D., and Ringwood, J.V. (2019). A critical comparison of excitation force estimators for wave energy devices. *IEEE Transactions on Control Systems Technology*.

Ringwood, J.V., Bacelli, G., and Fusco, F. (2014). Energy-maximizing control of wave-energy converters: The development of control system technology to optimize their operation. *IEEE Control Systems*, 34(5), 30–55.

Ringwood, J.V., Ferri, F., Ruehl, K., Yu, Y.H., Coe, R.G., Bacelli, G., Weber, J., and Kramer, M.M. (2017). A competition for wec control systems. In *Proceedings of the 12th European Wave and Tidal Energy Conference (EWTEC) 2017, Cork, Ireland*.

Ringwood, J.V., Mérigaud, A., Faedo, N., and Fusco, F. (2019). An analytical and numerical sensitivity and robustness analysis of wave energy control systems. *IEEE Transactions on Control Systems Technology*, accepted.

Tom, N., Ruehl, K., and Ferri, F. (2018). Numerical model development and validation for the WECCCOMP control competition. In *Proceeding of the 37th International Conference on Ocean, Offshore and Arctic Engineering, Madrid, Spain*, V010T09A042–V010T09A052.

Wave Star (2019). `http://wavestarenergy.com/`. Accessed: 24-Oct-2019.

WEC-Sim (2019). Wave Energy Converter SIMulator. `http://wec-sim.github.io/WEC-Sim/index.html`. Accessed: 11-Nov-2019.